Al-Imam Muhammad ibn Saud Islamic University

College of Science

Department of Chemistry

Synthesis and Photocatalytic Properties of Photoactive Systems

BaO, ZnO, ZnBaO and ZnBaCaO

A graduation research project

submitted to the Department of Chemistry in partial fulfillment of the requirements for the completion of the degree of Bachelor of Science in Chemistry

By

Fahad Hassan Al-sairy

Under supervision

of

Dr. A. A. HOUAS

Second Semester, May 2015

i

TABLE OF CONTENTS

LIST OF TABLES

LIST OF FIGURES

ACKNOWLEDGMENTS

الحمد لله الذي أعاننا على إنجاز هذا العمل على أحسن وجه

I would like to sincerely express my thanks to everyone that helped me. My special thanks to my supervisor, Dr. Ammar Ahmed Houas Professor at the College of Sciences. I also present my respects and thanks to Dr. Omar Khalid Al-duaij, Head of the Chemistry Department, Vice-Dean for Institute of History of Islamic-Arab Sciences and Dr. Abdulrahman G. Alhamazani, Vice-Dean for Quality and Development-College of Sciences, Deanship of Preparatory Programs - IMAM University for facilitating this work by providing the necessary guidances.

Thanks to my classmate, Muhamed Babetin for the discussion during report writing. I also would like thank Dr Lotfi Hedi Khezami and Dr Abuelez Khalid for providing me material, and I also would like to thank all my teachers for the help and chemical laboratory.

Last, many thanks to my family friends for the encouragement during the whole project.

ABSTRACT

Pure zinc oxide, pure barium oxide, (Ba) barium doped and (Ba, Ca) barium, calcium co-doped ZnO photocatalysts were prepared co-precipitation method using zinc nitrate, barium and calcium chloride in presence of oxalic acid at 60 °C and ammonium hydroxide concentrated solution. In the present project the effect of Barium doping and Barium, calcium co-doping on structural and morphological properties were investigated. Structural characterization by X-ray diffraction reveals that BaO pure has a cubic structure with the smallest crystal size and ZnO pure, ZnBaO and ZnBaCaO are polycrystalline with wurtzite structure and the particle size increases with doping. SEM images showed that Ba doping influenced surface morphology. ZnO pure grains are rather dispersed and much more agglomerated. Ba Doped and Ba, Ca co-doped ZnO grains are rather heterogeneous with the appearance of a new sticks shape in the case of ZnBaO. Analysis by BET method of the surface and porosity shows that the isotherms of all prepared samples are of type II, indicating the presence of mesopores (30-100 Å), indicating a rapid increase of porosity at 300 Å characterizing macropores with small hysteresis behavior. Adsorption reaction of Malachite Green (MG) follows the Lagergren pseudo first order kinetic band obeys to Langmuir model. Visible photocatalytic degradation is first order kinetic and the highest photoactivity was found with the ZnBaO photocatalyst (14 times higher than for the other prepared photocatalyts) .

Keywords: Zinc Oxide, Barium, Calcium, Physicochemical Properties, Adsorption, Photocatalysis Tests

مستخلص

أعدت الحفازات الضوئية التالية: أكسيد الزنك النقي وأكسيد الباريوم النقي و أكسيد الزنك المنشط بالباريوم و أكسيد الزنك المنشط بالباريوم والكالسيوم معا بطريقة الترسب المشترك و ذلك باستخدام نترات الزنك وكلوريد الباريوم وكلوريد الكالسيوم في وجود حمض الأوكساليك السخن الى 60 درجة مئوية بإضافة محلول هيدروكسيد الأمونيوم المركز . في المشروع الحالي تمت دراسة تأثير المنشطات الباريوم و تشارك الباريوم والكالسيوم على الخصائص الهيكلية والشكلية لأكسيد الزنك. توصيف الهيكلية التي حيود الأشعة السينية تكشف عن أن وأكسيد الباريوم النقي لديه بنية مكعب مع أصغر حجم للجسيمات بالمقارنة للحفازات الضوئية المحضرة الأخرى. أما بالنسبة لأكسيد الزنك النقي و أكسيد الزنك المنشط بالباريوم و أكسيد الزنك المنشط بالباريوم والكالسيوم معا (ZnBaO وZnBaCaO) فهي كريستالات الشكل في هيكل wurtzite كما لوحظت زيادة في حجم الجسيمات مع وجود المنشطات. وأظهرت تحاليل مجهر المسح الإلكتروني (SEM) أن وجود المنشطات أثرمورفولوجيا على سطح أكسيد الزنك بحيث أن بأكسيد الزنك النقي الحبوب متفرقة نوعا ما، وأكثرتكتل أما بأكسيد الزنك النشط بالباريوم وبتشارك بالباريوم والكالسيوم فالحبوب غير متجانسة مع ظهور شكل جديد (عصي) في حالة ZnBaO. التحليل السطح والمسامية باستخدام طريقة BET يدل على أن أيسوثرم جميع العينات التي أعدته هي من نوع II، مشيرا إلى وجود متوسط المسام mesopores (100-30 نانومتر) مع hysteresis صغير جدا. تفاعل إمتصاص الملكيت الاخضر (MG) يتبع نظام Lagergren المتمثل في حركية من الدرجة الأولى كما أن نظام الإمتصاص يطيع نموذج Langmuir. حركية التاكل الضوء تحفيزي للملكيت الاخضر تحت الإشعاع المرئي هي من الدرجة الأولى كما ان الحفاز الضوئي هو صاحب الفاعلية الضوء تحفيزية الأكبر (حوالي 14 مرة أكبر من الأخريات)

كلماتالبحث أكسيدالزنك،الباريوم،الكالسيوم،خصائصفيزيائية،الامتزاز،اختباراتضوئي

CHAPTER 1
INTRODUCTION AND RESEARCH OBJECTIVES

"Saudi Arabia's agricultural development over the last three decades has been astonishing. Large areas of desert have been turned into agricultural fields - a major accomplishment in a country that receives an average of about four inches of rain a year, one of the lowest rates in the world. As a result, there has been a phenomenal growth in the production of all basic foods. Saudi Arabia is now completely self-sufficient in a number of foodstuffs, including meat, milk and eggs. Water, of course, is the key to agriculture in Saudi Arabia. The Kingdom has successfully implemented a multifaceted program to provide the vast supplies of water necessary to achieve the tremendous growth of the agricultural sector.

A network of dams has been built to trap and utilize precious seasonal floods. Vast underground water reservoirs have been tapped through deep wells. Desalination plants have been built to produce fresh water from the sea for urban and industrial use, thus freeing other sources for agriculture. Facilities have also been put into place to treat urban and industrial runoff for agricultural irrigation.

An expanding source of water is the use of recycled water. The Kingdom aims to recycle as much as 40 percent of the water used for domestic purposes in urban areas. To this end, recycling plants have been built in Riyadh, Jeddah and other major urban industrial centers. Recycled water is used for irrigation of farm fields and urban parks"[1].

Furthermore, in 2010 the total municipal water demand in KSA was about 2863 million m^3 approximately 70% for industrial need [2]. Due to the high population growth and increased standard of living the domestic water demand have increased from 200 million m^3/year in 1970 to about 2063 million m^3/year in 2010 [3].

Effective ways to degrade molecules responsible of the aqueous pollution, allowing the recycling of wastewater, currently occupy a special place in the activities of scientific research. Photocatalysis, one of the famous Advanced Oxidation Processes (AOPs), has proven an attractive route for the purification of contaminated water. This method uses the photon energy to catalyze chemical reactions. Applications include decomposition of water into hydrogen and oxygen [4] and the complete oxidation (mineralization) of organic contaminants in the aquatic environment. [5]

In recent years, catalysts such as TiO_2, ZnO, WO_3, SnO_2 [6,7], $ZrO2$ [8], Nb_2O_5, CdS and ZnS [9] were used as oxidation photocatalysts of organic contaminants. Among these

materials, ZnO has been found to be an excellent photodegradation catalyst [8.10- 12,15]. It has good chemical stability in addition to its low cost. [13] However, the energy of the band gap (3.37eV) involves only 5% of the solar spectrum [6, 8, 9, 14]. Furthermore, the fast-electron hole recombination is a limiting factor for the effectiveness of the catalyst [10,14]. Doping ZnO with cations with the same valence of zinc may have a double effect:

- reduction of the energy of the gap, which has to effect of the displacement of the absorption in the visible region;
- reduction of the electron-hole recombination.

Recent work concerns the doping of ZnO by transition metals [10, 12,15], and alkaline earth metals and obtaining mixed oxides such as $SrTiO_3$ [9,16- 18]. The results continue to be the subject of discussion.

Regarding all reasons mentioned above, comes the purpose of this project which will be based on:

☐ Objectives and research questions:

- Research Objectives: The main objective of this research is the preparation and characterization of pure and Barium or/and calcium doped zinc oxide. A second objective is to study the adsorption phenomena of Malachite Green (MG) on the prepared samples. A third objective is to test these photocatalysts on the visible degradation of MG and to try to find correlations between their activities and their physicochemical.
- Research Questions: **<u>Question1</u>**: What are the conditions for preparing and crystalline phases obtained with Zinc oxide when doping with barium? **<u>Question 2</u>**: Is there a link between the preparation and the adsorptive properties, the state of division of the catalysts obtained and the chemical nature of Zinc substitution by the Barium cation? **<u>Question3</u>**: What photocatalytic performance are those solid when varying the matrix containing the Zinc?

☐ Methodological Consideration and Content:

The present work has requested, in a first step, a literature survey in the field of the synthesizes of semiconductors and the heterogeneous photocatalysis.

In a second step, attempts to obtain Zinc oxide and doped zinc oxide are undertaken to develop a simple and reproducible surgical protocol.

In a last step, the solids obtained are characterized and tested in photodegradation of Malachite Green (MG) to identify correlations among the physical and chemical properties identified and photocatalytic performance.

Thus, the content of this manuscript is divided into three chapters:

- The first chapter refers to a literature study on pure and doped zinc oxide: some ZnO characteristics, synthesis methods of pure and doped zinc oxide and their applications and heterogeneous photocatalysis principle .

- The second chapter deals with methods and materials used in this project: synthesis method and some characterization techniques .

- The third chapter focuses on the obtained results and their interpretations and discussions.

CHAPTER 2
LITTERATURE REVIEW

2.1. Physico-chemical properties of zinc oxide ZnO

In nature, ZnO is in the form of an orange-red mineral called zincite (Figure.2.1). The red color of the natural mineral is due to the presence of impurities (Fe^{2+}, Mn^{2+}), however zincite is extremely rare and its operation is very limited. It is also an abundant by-product of zinc metallurgy. Generally from the oxidation of the main zinc ore, sphalerite (zinc blende, ZnS) or recovery of industrial waste, it is in the form of an amorphous white powder.

Zincite crystals   ZnO powder

Figure.2.1 Zinc oxide Image as crystals zincite and white powder

2.1.1 A Brief History of ZnO

The first publication on zinc oxide goes back to 1935 when C.W. Bunn determined the parameters of the mesh, and then, in 1960 D.G. Thomas was able to study this material as a semiconductor by determining its reflectivity, absorbance and energy of excitons (59 meV) [19, 20]. Due to these works, which are still references, this semiconductor was the first oxide used as photocatalyst in the oxidation of carbon monoxide by Haufe in 1964 [21]. Since this time zinc oxide was the subject of thousands of publications to understand his promising properties. With its wide band gap 3.37 eV (stoichiometric and at room temperature) and wide energy excitons, ZnO is distinguished by its light absorbance, piezoelectricity, ferromagnetism, thermochromy, hardness and stability .., to be applied in paints, plastics, rubber manufacturing, pharmaceuticals, cosmetic products, electricity ... etc. [22]. ZnO has also been part of the nanotechnology world, especially from the nineties, in the development

of nano-devices such as photovoltaic, transistors, diodes, nanosensors and photocatalysts ... etc.

2.1.2 Crystallographic properties of ZnO

Depending on the preparation conditions, zinc oxide exists under three different structures. The first structure is the hexagonal wurtzite, stable under ambient conditions; the second is the unstable cubic structure which appears at elevated pressures; the third is the Rock-Salt structure that forms under very high pressures (Figure.2.2) [23-25]. In our present study we are interested in developing under ambient conditions so to the hexagonal wurtzite structure.
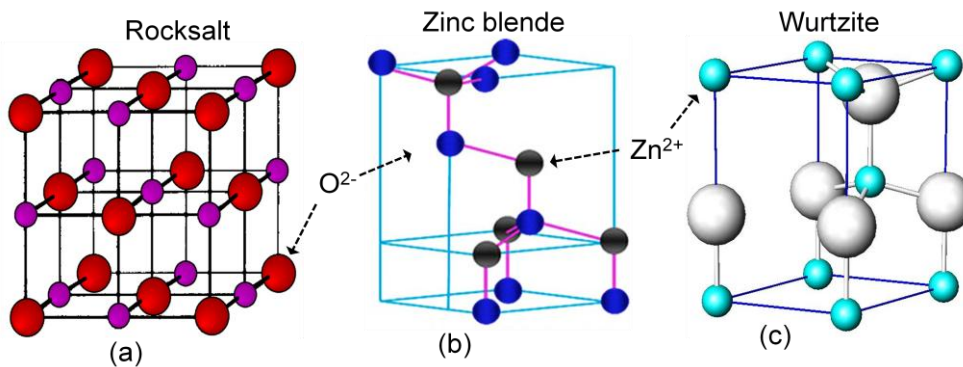
Figure.2.2: Crystal structures of ZnO; (a) Cubic Rocksalt, (b) Cubic Zinc blende and (c) Hexagonal wurtzite.

In the ambient conditions, the ZnO crystallizes in a hexagonal wurtzite-type network (P63mc), wherein the oxygen O^{2-} ions are arranged in a hexagonal close-packed type network, and where the zinc ions Zn^{2+} occupy half tetrahedral interstitial position with the same arrangement as the oxygen ions (Figure.2.3) [23, 26]. The wurtzite structure contains four atoms per cell whose positions are: [37] O^{2-} [(0, 0, 0), (2/3, 1/3, 1/2)] and Zn^{2+}: [(0, 0 3/8) (2/3, 1/3, 7/8)].
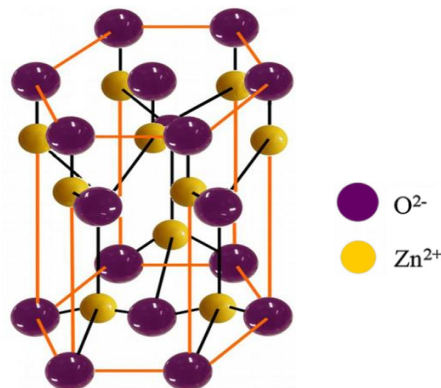
Figure 2.3: Hexagonal wurtzite structure of ZnO

In fact, the environment of each ion does not have exactly tetrahedral symmetry. Indeed, the distance between the nearest neighbors in the c direction is smaller than the other three neighbors. This is the origin of the ZnO pyroelectricity. Each zinc atom is surrounded by four oxygen atoms and vice versa. It is said that the coordination number is 4: 4. Indeed, the zinc atom is not exactly in the center of the tetrahedron but displaced by 0.11 Å in a direction parallel to the c axis. Oxygen molecules therefore continue, to some extent, their individuality, contrary to what one would expect from a purely ionic crystal. Hexagonal mesh of the wurtzite structure is characterized by three lattice constants **a**, **c** and **u**; **a** is the side of a lozange constituting the base, **c** is the side parallel to the Oz axis and **u** is an internal coordinate along this axis. These constants determine the relative position of subnets O^{2-} anion and cation Zn^{2+} (Table.2.1).

Table.2.1: Summary of the characteristics of the crystal structure of ZnO [27]

Lattice		**Hexagonal Wurtzite**
Distance between O^{2-} and Zn^{2+} (nearest neighbors)		a = 3,2499 Å $\rightarrow$ c/a = 1,6019 c = 5,2060 Å ; u = 0,345
Ionic radius for a tetrahedral coordination	Covalent bond Ionic bond	neutral Zn = 1,31 Å, neutral O = 0,66 Å Zn^{2+} = 0,60 Å, O^{2-} = 1,38 Å
Crystallin radius for a tetrahedral coordination		Zn^{2+} = 0,74 Å O^{2-} = 1,24 Å

The coordinate u is defined by the following relationship:

$$u = ¼ + (c^2/3\ a^2)$$

Based on this relationship, we note that the parameter u is dimensionless. The distance between the index lattice planes (h, k, l) is given by the relation:

$$\frac{1}{d} = \frac{c^2}{3a^2} + (h^2 + hk + k^2) + \frac{l^2}{c^2}$$

The stability condition of this structure is given by the following equation:

$$0,225 \leq \frac{R_{an}}{R_{cat}} \leq 0,414$$

R_{an} and R_{cat} are respectively the radius of the anion and the cation.

From the values of the cation and anion ionic radius shown in Table 2, it can be noted that the structure of ZnO is relatively open. Indeed, the zinc atoms and oxygen occupy only 40% of the crystal volume, leaving empty spaces with radius of 0.95 Å. It is possible that, in certain conditions, excess zinc atom can take place in these spaces in interstitial position. These characteristics help to explain some particular properties of the oxide, related to the phenomena of semiconductivity, photoconductivity, luminescence, as well as chemical and catalytic properties of the solid [27].

2.1.3 Crystallographic properties of ZnO

With sufficient crystalline quality, zinc oxide lets up to 80% of visible light and that is why it is now used as a transparent conductive oxide whose refractive index in the form mass is equal to 2 [28]. However, it is within the class of so-called conductive transparent oxides TCO (transparent conductive oxides) only when it is doped. Very lightly doped, it can be used in luminescence. The visible luminescence of ZnO is due to defects in emission levels deep (virtual levels between the conduction band and the valence band), as the interstitial zinc and oxygen vacancies [29].

As optical properties, electrical properties of ZnO are evaluated according to defects caused by the surface state of the material. Thus, more ZnO has impurities, more they cause diffusion of charge carriers.

Finally, we can say that zinc oxide is exceptionally rich in many optical, electrical and mechanical properties that depend on its morphology and its surface condition.

2.2. Application of ZnO photocatalysis

Since 1960, ZnO is often considered a valid analogous to TiO_2 (the most famous semiconductor in photocatalysis) because of these good optoelectronic properties, catalytic, photochemical besides low cost [21]. Due to the position of the ZnO valence band, photogenerated holes have a strong oxidizing power, sufficient to break down most organic compounds. [30] ZnO has been tested in the decomposition of aqueous solutions of various dyes [31-36], and many other environmental pollutants [37-40].

In many cases, ZnO has been reported to be more effective than TiO_2 [37-40]. However, the discovery of ZnO photocorrosion and its chemical sensitivity to extremes conditions of pH, limit significantly its application in photocatalysis. [41]

Kislov et al. showed that the photoactivity and photostability some samples of single crystal ZnO are highly dependent on the crystallographic orientation [42].

7

Several studies have shown that ZnO is very active under visible light in the photo-degradation of certain organic compounds in aqueous solution [36, 43]. Methyl green was discolored and degraded successfully by ZnO under visible irradiation with low intensity. The addition of an oxidant ($Na_2S_2O_8$ or H_2O_2) improves the pollutant degradation rate [44]. Lu and col. used ZnO for the degradation of the Blue 11 under visible irradiation and studied the effects of the factors influencing the performance of the photocatalytic reaction as the initial concentration of the dye, the dose of the catalyst and the initial pH [45]. Pare and col. have shown that addition of an optimal amount of hydrogen peroxide and potassium persulfate increases the photocatalytic degradation of acridine orange, while the yield was greatly decreased by the addition of inert salts such as NaCl and Na_2CO_3 [46]. Sakthivel and col. studied the photodegradation under sunlight of Brown acid 14 as a pollutant model to evaluate the photocatalytic performance of ZnO and TiO_2. The highest photodegradation rate was observed for the ZnO, suggesting that it absorbs a large fraction of the solar spectrum and absorbs more light than the TiO_2 [47]. Pardeshi and Patil confirmed that by using ZnO, phenol degrades more effectively under sunlight than under artificial visible light. Moreover, ZnO was reused five times and suffered low photocorrosion, so in these working conditions there is a negligible risk to be taking into account [48]. ZnO has rarely been tested as a photocatalyst in the gas-solid field despite it was found more active than the commercial TiO_2 and synthesized for the photo-decomposition of acetic acid [196]. Furthermore, by comparing them to a shopping ZnO powder, ZnO nanoparticles high surface area showed a higher photocatalytic activity in the degradation of a hard gaseous pollutant such as $(CH_3)_2S_2$ [49]. El-Kemary and col. synthesized ZnO nanoparticles by heating a mixture of zinc acetate dihydrate and triethylamine in ethanol for 60 min at 50-60◦C. The photocatalytic activity in the degradation of ciprofloxacin was studied under UV light irradiation. The degradation process was effective at pH 7 and 10, but rather slow at pH 4 [50]. ZnO prepared by Colon and col. from zinc acetate and triethylamine as template by precipitation, sol-gel and other treatments hydrothermals shows high conversion values of the photooxidation of phenol. An additional heat treatment results in higher conversions than those obtained with Degussa P25 [51]. ZnO nanostructures obtained by thermal decomposition of zinc oxalate without using additives or solvents was more effective than the commercial ZnO in mineralization of Red 120 under solar irradiation [52]. Kitture and col. prepared polydisperse ZnO nanoparticles with a particle distribution in two different sizes (30 and ~ 120 nm). The samples were tested in the degradation of methylene blue and methyl orange under sunlight.

ZnO nanowires at high level of alignment and uniformity were prepared by deposition process on substrates of indium oxide and tin by using a microwave. [53]. The nanotubes were effective for the degradation of BM under UV irradiation and presented a very dependent activity to their size. Hierarchically porous spherical ZnO nanoparticles showed higher than photoactivity of TiO_2 in the degradation of phenol [54]. Nano-ZnO flowers were more effective than nanotubes in the degradation of 4-chlorophenol under UV irradiation [55]. The superior performance of ZnO nanoflowers result due to oxygen vacancies on the surface of nanomaterials 1D. Recently Zongbao and col. prepared nanoparticles of ZnO doped with substitutional nitrogen by calcining ZnO semicrystalline at 400 ° C under ammonia gas. While similar nitrogen doping ZnO crystalline nanoparticles cannot be obtained. The results showed that the photoactivity of ZnO in the degradation of Rhodamine B under visible irradiation increased due to N2p states in the band gap. [56]

2.3. Synthesis of photocatalysts

Methods and conditions of synthesis of photocatalysts materials are the first tools influencing the photocatalytic performance by controlling material surface properties directly. Today, there are dozens of methods used in a laboratory scale or industrial. However, the choice of method should be based on key criteria, namely, simplicity coupled with the lowest cost, speed and control of surface properties.

Based on these criteria, we chose to synthesize our front photocatalysts with the co-precipitation method.

2.3.1. The co-precipitation method

The term co-precipitation refers to the precipitation reaction of two or n metal salts in the same solution. The reaction is conducted simply by adjusting the pH. The obtained precipitate is filtered, dried and then thermally decomposed. The precursor so formed is calcined at temperature sufficient for the crystallization of the solid. There are four types of co-precipitation: the surface adsorption, the formation of mixed crystals, occlusion and mechanical trapping [57]. The surface adsorption and the formation of mixed crystals are equilibrium processes, while the occlusion and mechanical trapping result from the crystal growth conditions.

   - Surface Adsorption is a process in which a soluble electrolyte returned from the solution to the surface of a coagulated colloid. This compound consists of an ion adsorbed in the primary layer and an opposite charge ion in adjacent layer populated by the against-ions.

- The formation of mixed crystals is a type of co-precipitation where contaminant ions replace the lattice ions.

- Occlusion is a type co-precipitation where undesired compound is trapped in the interstitial cavities caused by rapid crystal growth.

Co-precipitates impurities may be the result of positive and negative errors. If the contaminant is not a compound of the element to be assayed, the result is always positive errors. In the other hand, if the contaminant contains the element to be determined, one can observe positive errors and negative. The presence of impurities in the final product remains the major drawback of this method, but this problem can be solved by proper washing consisting to wash the precipitates until the complete elimination of all impurities.

In the present work we have chosen the co-precipitation technique for the preparation of some photocatalysts ZnBaO and ZnBaCaO. This is a simple method that has attracted a lot of attention to the high homogeneity and purity of the final product more than the vast kinetics of precipitates forming reaction. Species frequently used in this method are hydroxides, oxalates and carbonates.

Recently, Hamrouni and col. [58-61] articles HAMROUNI] have dominated research on ZnO-SnO$_2$ photocatalysts prepared by co-precipitation. They studied the effect of several operational parameters on the degradation of some dyes. They showed that under UV irradiation, the photocatalytic activity of ZnO coupled with 50% SnO$_2$, is larger compared with that of ZnO and SnO$_2$ pure.

2.4. ZnO photocatalytic performance improvement

ZnO is a type of semiconductor " n " i.e. that basically, electrons are the majority carriers and holes are the minority carriers. Until the 90s scientists have explained this phenomenon by the contribution of oxygen vacancies and interstitial zinc atoms in the conductivity [62-64]. However, recently, several studies have shown that it not really true. Although the oxygen vacancies training energy is lowest among those funds defects, density functional calculations indicate that a deficiency of oxygen is deeper than a shallow donor or surface, therefore, it cannot contribute to an n-type conductivity [65-67]. Similarly, the interstitial zinc is unlikely to be responsible for the n-type conductivity because it will be present in very low concentrations in the n-type ZnO. [68] The most correct theory so far, including wholes scientists are in agreement, is the effect of impurities. Attendance of these in the crystal lattice of ZnO changes dramatically these optical and electrical properties.

In photocatalysis doping ZnO is a very beneficial tool to shift its absorbance to the visible range, therefore, specifically to reduce the energy of the Fermi level and stop recombination. On the other hand, if the electrons transferred to the conduction band react directly before they are recombined with the holes, the photocatalytic performance will be at the highest level. But, the speed of the recombination reaction is still faster. Thus, the presence of a second conduction band energy more or less below the first allows electrons to be transferred before they are recombined. This is called the coupling of metal oxides.

2.4.1 Doping ZnO

- *p doping*

P-doping of ZnO can be done at the site of Zn deficiencies by adding elements of AI Group: Li, Na, K, Cu, Ag It is also possible by adding the AV group elements in the gaps. O sites such as:. N, P, As The p-doped ZnO is very difficult and remains a challenge and an indispensable component of the development of ZnO [69].

- *n doping*

The doping elements n ZnO are components of AIII group of the Periodic Table such as Al, Ga, In substituting Zn. Or elements of AVII group such as Cl, I substituted into oxygen sites.

2.5. Semiconductor photocatalysts

Due to the possibility of producing electron- hole pairs, some semiconductor (TiO_2, ZnO, WO_3, SnO_2, CdS etc.) may be the site of a oxido-reduction reaction initiated by light. When a photon of energy (E) greater than or equal to the energy of the band gap (Eg) is absorbed by a semiconductor (SC), an electron (e^-) is promoted from the valence band (BV) to the conduction band (BC) (equation 1). This electron leaves behind in the BV a hole (h^+). The electron and the hole are two electronic species, respectively highly oxidant and reducer. These are the charges that will allow redox reactions at the semiconductor surface.

$$SC + h\nu \rightarrow h^+_{BV} + e^-_{BC} \tag{1}$$

If during its movement the electron returns to its original level of valence, it is called direct recombination of electron / hole (e^- / h^+). This is the width of the forbidden energy band (Eg) between the valence and conduction bands will determine what wavelength of light radiation, semiconductor can absorb. [70] We must have $h\nu \geq Eg$; which means that the wavelength must satisfy the relationship: $\lambda \geq hc / Eg$

2.5.1. Principle of the photocatalysis

As any catalytic reaction, a photocatalytic reaction can be conducted in aqueous, gaseous or liquid organic media [71]. The principle of photocatalysis based on the same five steps of catalysis:

1. Transfer of molecules of the liquid or gas phase to the surface of the photocatalyst,

2. Adsorption of reactive molecules on the surface of the photocatalyst,

3. Photocatalytic Reaction in adsorbed phase,

4. Desorption of the reaction products,

5. Transfer of the reaction products from the boundary layer of the photocatalyst to the liquid or gas phase.
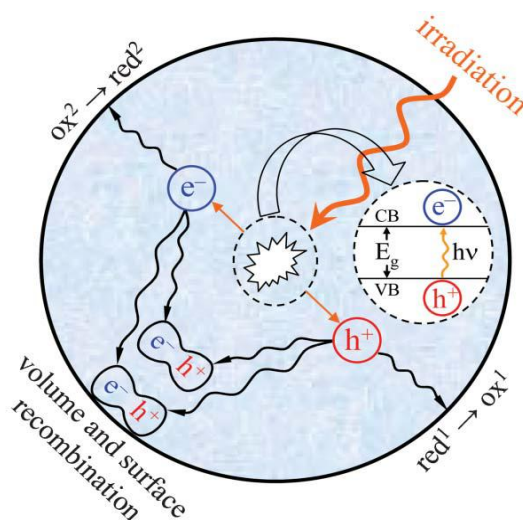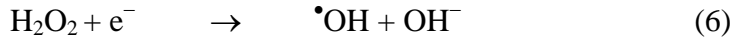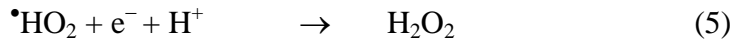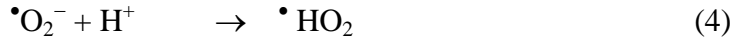

Figure 2.4: Representation of a semiconductor photocatalyzed reaction. [72]

We can consider that the photocatalysis is an exceptional case of catalysis. This exception occurs in the complication of the photocatalytic reaction that is triggered following the training of pair e^-/h^+ in response to photoexcitation of the catalyst (Figure.2.4). These peers are redox species and considering that their production is the first parameter of the referential photocatalytic activity of such irradiated semiconductor. On the other hand, during formation of e^-/h^+ pair, the catalyst adsorbs spontaneously across its boundary layer several other molecules according to their redox potential such as water, oxygen and reactants. Therefore, the surface of the catalyst will be the seat of the oxidation and reduction reactions between adsorbed molecules and pairs e^-/h^+ to produce other oxidizing molecules and has a powerful response. Initially there will be reduction of oxygen and oxidation of water adsorbed to produce radical respectively $^\bullet O_2^-$ and hydroxyl radical $^\bullet OH$:

$$O_2 \text{ }_{(ads)} + e^- \rightarrow {}^\bullet O_2^- \qquad\qquad\qquad (2)$$

$$H_2O + h^+ \rightarrow {}^\bullet OH + H^+ \qquad\qquad\qquad (3)$$

Thus, there will be the creation of other oxidizing and very reactive species:

$${}^\bullet O_2^- + H^+ \qquad \rightarrow \quad {}^\bullet HO_2 \qquad\qquad\qquad (4)$$

$${}^\bullet HO_2 + e^- + H^+ \qquad \rightarrow \qquad H_2O_2 \qquad\qquad (5)$$

$$H_2O_2 + e^- \qquad \rightarrow \qquad {}^\bullet OH + OH^- \qquad\qquad (6)$$

$$H_2O_2 + h\nu \qquad \rightarrow \qquad 2{}^\bullet OH \qquad\qquad\qquad (7)$$

$$H_2O_2 + {}^\bullet O_2^- \qquad \rightarrow \qquad OH^- + H_2O + O_2 \qquad (8)$$

The whole of all these species will lead therefore to the formation of intermediate products and finally total mineralization molecules adsorbed on the surface. However, it should be noted that among all the formed oxidizing species, the hydroxyl radical (${}^\bullet OH$) is one the most powerful oxidizing agent known [73]. It has a redox potential of 2.73 V / ENH in acid solution [74]. In strong alkaline medium, the radical ${}^\bullet OH$ exist under its basic form, the oxygen radical anion ${}^\bullet O^-$ (pKa = 11.9) reacting with nucleophilic attack [71]. When the pH are more acidic, the acid form is predominant and reacts with the adsorbed molecules by electrophilic attack:

$${}^\bullet OH + OH^- \qquad \rightarrow \qquad {}^\bullet O^- + H_2O \qquad\qquad (9)$$
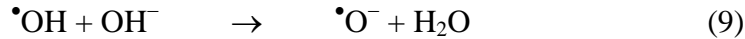
The half-life of the radical ${}^\bullet OH$ is estimated to less than 70 ns in water [74]. The reaction rates Of ${}^\bullet OH$ radicals and organic compounds are very fast, of the order of 10^6-10^{10} M.s^{-1} [74].

The reaction intermediates are formed either by reacting with pair e^-/h^+ or largely with the reactive species formed:

$$R\text{-}H + {}^\bullet OH \quad \rightarrow \quad R^\bullet + H_2O \quad / \quad R + h^+ \rightarrow R^\bullet \qquad (11)$$

$$nR\text{-}OH + m{}^\bullet OH \quad \rightarrow \quad \text{intermédiaires} \quad \rightarrow \quad pCO_2 + aH_2O \qquad (12)$$

Chapter 3
Materials and Methods

3.1. Introduction:

The preparation of photocatalysts is an essential step in almost all applications in heterogeneous photocatalysis. Nevertheless, the photocatalytic performance is based on several surface properties such as crystallinity, photosensitivity, specific surface, etc ... So it is necessary to study the correlation between photocatalytic efficiency and physicochemical properties of photocatalysts in order to interpret and evaluate the results of photocatalytic reactions.

In this context, this chapter presents the characterization techniques and equipment used in order to gather as soon as possible information on the surface properties of the prepared photocatalysts. The latter, it was analyzed by X-ray diffraction (XRD), the specific surface area analyzer using the technique of Brauner-Emmet-Teller (BET), and scanning electron microscopy (SEM).

3.2. X-ray diffraction (XRD)

In order to determine the crystal structure and the particle size of the synthesized photocatalysts, XRD analysis have been developed using Bruker-AXS D8 diffractometer and Ital Structures ODA 2000. All analyzes at room temperature was carried out with the CuKα radiation for 30 kV and 30 mA.

The ray diffraction technique X (also called X-ray crystallography) is based on Bragg's law:

$$n\lambda = 2\ d\ Sin\theta$$

With:

n: diffraction order

λ: wavelength

d: lattice spacing

θ: diffraction angle

The monochromatic X-radiation is produced by an anticathode average atomic number (eg. Cu, Mo) excited to the optimum transmission voltage characteristic of the radiation, a filter or a monochromator selects the Kα line. The sample is polycrystalline. Assuming that the irradiated part of the preparation contains a very large number of crystallites in perfectly disorientation statistics, there are still a number of them having at beam a family of planes (hkl) given at an incidence θ compatible with reflection selective order n which is expressed by the Bragg condition.

Vesting conditions are a 2θ angle range from 10 ° -80 °. The positions and intensities of the various diffraction lines observed were compared to those available in the data bank of the reference sheets JCPDS (Joint Commitee Powder Diffraction Standards)

The particle size was estimated using the equation of Debye-Scherrer:

$$D = (0.9\lambda) / (\beta \cos\theta)$$

Where D is the particle size (nm) λ is the radiation ray of the wavelength X (0.154 nm), β is the width at half height of the main peaks and θ is the Bragg angle in (radian).

3.3. Specific Area and Porosity

Generally, the specific surface area of a material corresponds to the total area per unit mass. Its determination is based on the adsorption of a certain gas at low temperature according to the method of Brunauer, Emmett and Teller (BET). This method consists of measuring of the volume of gas adsorbed in a complete monolayer on the surface of a sample at a temperature equal to -196 ° C.

Nitrogen adsorption and desorption measurements were performed at liquid nitrogen temperature (-196 °C) on a Micromeritics ASAP 2010. The samples were outgassed in vacuum at 200 °C for 20 min before measurements

3.4. Scanning electron microscopy (SEM):

Scanning electron microscopy images are formed sequentially by scanning the sample surface and collecting emitted particles. Depending on the type of detected particles, the scanning electron microscope provides different images in which information may be complementary.

In fact, the surface atoms are jostled by an electron comers spring rain. Either the electron bounces off the atom as a ball on a ball (back scattered electron) or it excites the atom disrupting the electron cloud. In the latter case the de-excited atom rejects an electron. When it is found outside of the material, it is a "secondary electrons" that is slower and can be captured with a probe brought to a low positive potential. The quantity of these secondary electrons depends only on the angle of incidence of the beam: the more it is grazing, the more excited volume is large, so the production is more important. Hence the topographic contrast effect: well oriented slopes from the detector appear brighter while those who send their secondary electrons on the side opposite to that of the detector appear dark.

In order to have information on the morphology and SEM examination of the particle size were carried out using a Philips XL30 ESEM apparatus operating at 30 kV on samples covered with gold.

3.5. Photocatalysis Characterization

The characterization of the prepared semiconductors has been carried out using the reaction of degradation of dye model molecule: Malachite Green (MG) using a cylindrical photoreactor containing 500 ml of the MG solution (30 mg/L). For each photocatalytic reaction the amount of the photocatalyst was chosen to ensure the absorption of substantially all of the photons emitted by the suspension. The light source is a 20 W/865 LUMILUX daylight lamp (OSRAM DULUXSTAR, China) with peaks maxima at 435 nm (blue), 490 nm (blue/green), 545 nm (green), 587 nm (yellow) and 610 nm (orange) are visible resulting in white light [http://www.osram.com.au], positioned axially in the photoreactor. The temperature of the slurry was controlled by circulating water through a Pyrex cylinder surrounding the lamp. A magnetic stirrer was used to ensure homogeneity of the reaction mixture. Before the light was switch on, the suspension was kept in the dark for 1 hour to reach equilibrium adsorption-desorption. Samples were taken at different time intervals to assess the progress of MG degradation. Finally, each sample was centrifuged and the MG residual concentration was measured using an UV-Vis spectrophotometer (Shimazu .   )

3.6. Synthesizes Protocols

The co-precipitation method is based on precipitation reactions of two or more salts, generally inorganic, in the same aqueous solution.

The $Zn(NO_3)_2.6H_2O$ and $BaCl_2.2H_2O$ (Aldrich) corresponding precursors of ZnO and BaO pure, respectively, were used as starting materials. In all synthesizes, distilled water was used as a solvent and ammonium hydroxide NH4OH (28%, Sigma Aldrich) as the precipitating agent.

- To prepare the pure oxides, amount of $Zn(NO_3)_2.6H_2O$ or $BaCl_2.2H_2O$ salt was completely dissolved in 50 mL of distilled water, with vigorous stirring giving the solution **A**. Then the solution **A** was added to a solution **B** of 50 mL of oxalic acid (0.1 M) at 60 °C and vigorously stirred. The obtained mixture was titrated by a concentrated NH_4OH solution until pH 7.

- Ba doped and Ba, Ca codoped Zinc oxides were prepared using the same procedure but with solution **A** containing respectively $Zn(NO_3)_2.6H_2O$ and $BaCl_2.2H_2O$ amounts with molar ratio Zn/Ba = (99/1) % and $Zn(NO_3)_2.6H_2O$, $BaCl_2.2H_2O$ and $CaCl_2$ with Zn/(Ba+Ca) = (98/(1+1)) %.

- The precipitates thus formed were filtered and washed extensively with bi-distilled water and then dried in an oven at 110 °C 24hours. Finally, the obtained powders were crushed and calcined at 600 °C for 2 hours in air in a muffle furnace.

- The photocatalysts prepared are symbolized by ZnO pure, BaO pure, ZnBaO and ZnBaCaO.

Chapter 4
Results and Discussions

4.1. Synthesized photocatalysts characterization

4.1.1. XRD characterization

The X-ray diffraction patterns of BaO pure, ZnO pure, ZnOBa and ZnOBaCa photocalysts are shown in figure.4.1. The diffractograms of the samples reveals that for BaO pure, the major diffraction patterns are from cubic BaO however for doped ZnO samples, the structure of all the peaks are in good agreement with the JCPDS data belonging to hexagonal wurtzite ZnO structure (Card No. 36-1451). Also for theses samples, no peaks corresponding to either barium, barium oxide or other complex oxides were detected. This observation suggests that in these samples, ZnO is really doped with Ba or with Ba and Ca. Since no phase segregation or secondary phase formation are detected it can be considered that Ba as well as Ca are incorporated into the ZnO lattice.
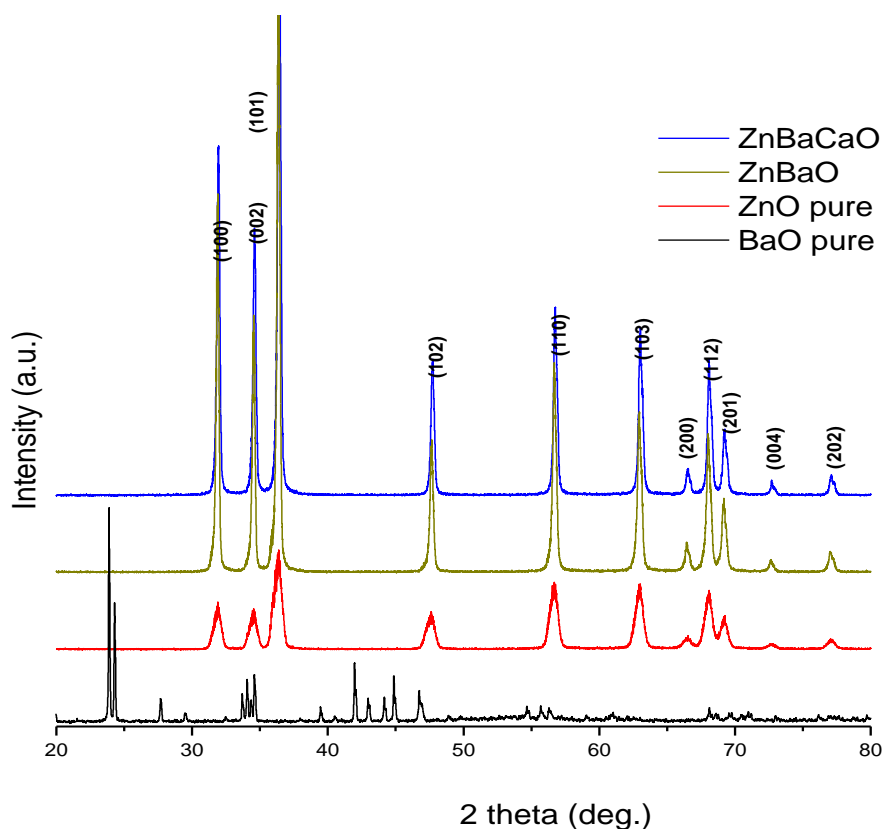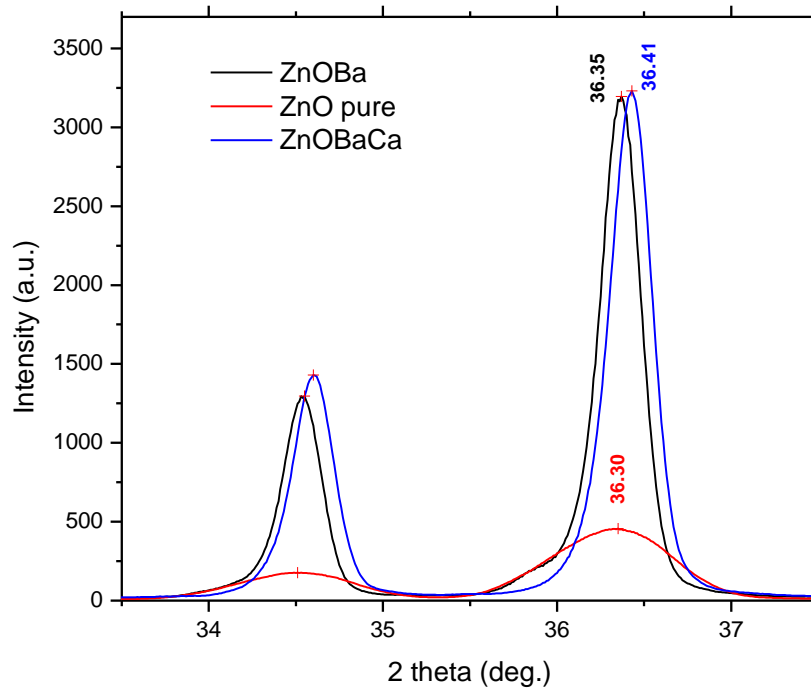

Figure 4.1. XRD patterns of ZnO pure, ZnBaO and ZnBaCaO photocatalysts

Figure 4.2 shows the changes in the 2θ angle values of the diffraction planes of (002) and (101) peaks at 2θ=33°-37°. It can be seen that ZnO pure, ZnOBa and ZnOBaCa grow preferential along (101) direction and the position of this peak shifted toward higher angle when doping. This shifting leads to the decreasing of d-spacing values as indicated in table 4.1. The intensity of (101) peak is found to increase when ZnO is doped with 1mol.% of Ba or co-doped with 1 mol.% of Ba and 1% mol. of Ca.

The diffractograms indicated that Ba^{2+} ions of the doped ZnO samples were only incorporated in the ZnO lattice. This is probably due to the difference between the ionic radius of Ba^{2+} (1.33 Å) and Zn^{2+} ion (0.74 Å). Since ionic radius of Ca^{2+} (0.99 Å) is smaller than that of Ba^{2+} its incorporation may be easier and facilitate by the presence of Ba^{2+}.

Figure.4.2 . XRD pattern at 2θ = 34°-37° of ZnO pure, ZnBaO and ZnBaCaO photocatalysts

The grain size, *D* of crystallites has been calculated using the well-known Debye Scherer's formula (1):

$$D = (0.9\lambda) / (\beta\cos\theta) \qquad \textbf{(1)}$$

where λ = 0.15405 nm is the x-ray wavelength, β is the peak width of half maximum and θ is the Bragg's diffraction angle.

The calculated values of particle size are given in Table.4. 1. It can be seen that, the crystallite size increases when ZnO is doped with Ba and co-doped with Ba and Ca.

Table4.1. Structural parameters of prepared photocatalysts

Samples	2θ (degree)	hkl	d-spacing (Å)	FWHM (degree)	Crystallite size (nm)	S_{BET} ($m^2.g^{-1}$)
BaO pure	24.35	(311)	3.652	0.557	15.51	14.51
ZnO pure	36.30	(101)	2.4728	0.356	28.96	4.51
ZnBaO	36.35	(101)	2.4695	0.114	89.35	1.45
ZnBaCaO	36.41	(101)	2.4655	0.11	90.49	5.82

4.1.2. Scanning Electronic Microscopy Analysis (SEM)

Figure.4.3 shows the SEM micrographs of BaO pure, ZnO pure, ZnBaO and ZnBaCaO photocatalysts. It can be observed that BaO sample is clearly different from the based zinc oxide samples. It is denser and its homogeneity is higher presenting closely packed spherical grains with almost the same shape. ZnO pure grains are rather dispersed and much more agglomerated. Ba Doped and Ba, Ca co-doped ZnO grains are rather heterogeneous with the appearing of a new sticks shape in the case of ZnBaO.

The undoped ZnO and Ba, Ca co-doped ZnO looked porous while the Ba doped ZnO are compact. This can be due to the fact that the incorporation of Ba in the starting solution improves the nucleation process. Agglomeration of small grains in certain regions of the solids is also evident from Figure.4.3 (b) and (d). Such agglomerations make difficult to evaluate the grain size from SEM images.
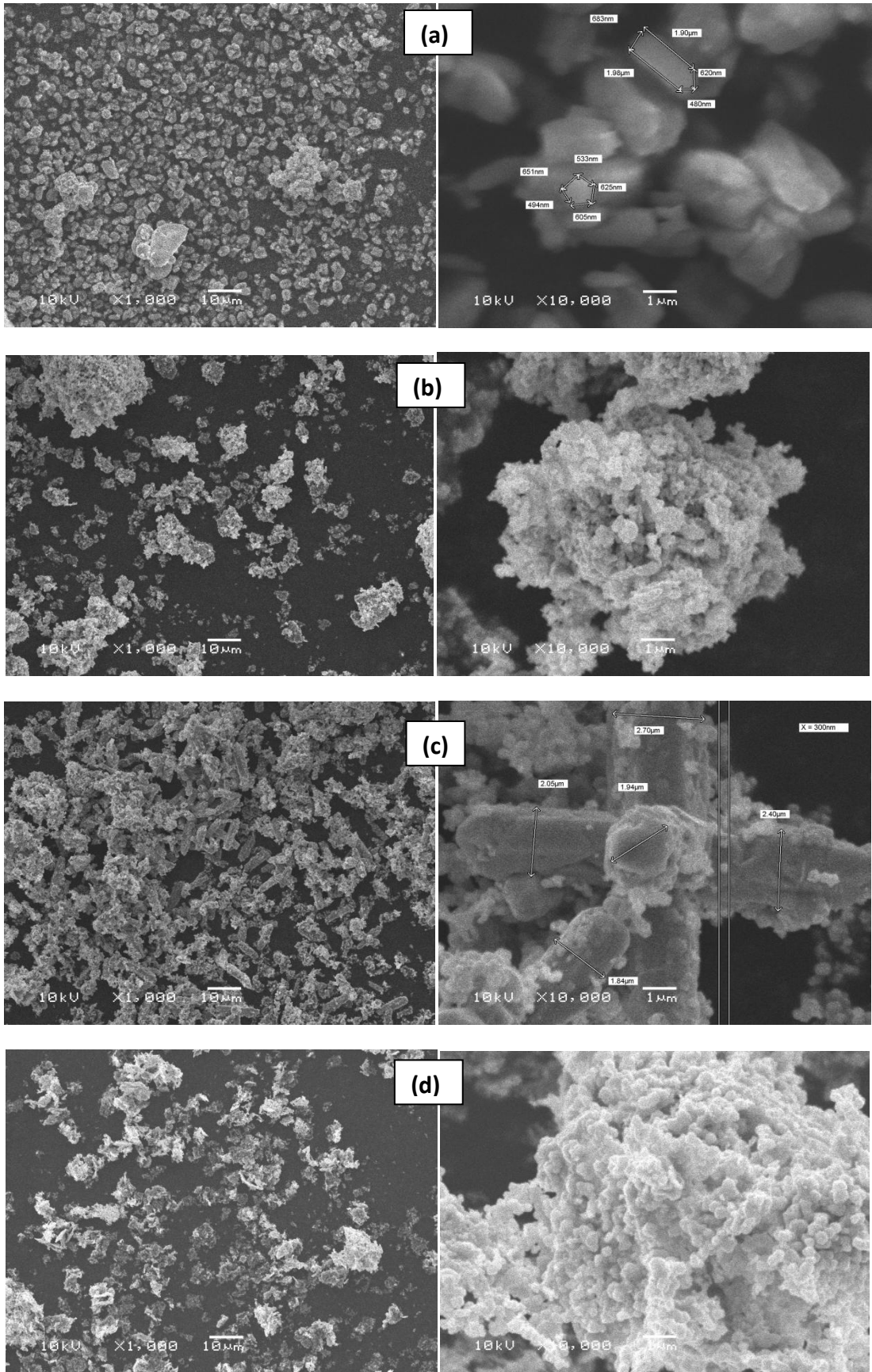
Figure.4.3. SEM images of(a) BaO pure, (b) ZnO pure, (c) ZnBaO and (d) ZnBaCaO photocatalysts

4.1.3 Brunauer–Emmett–Teller (BET) surface area and pore size distributions

Figure 4.4 (a) and (b) shows the nitrogen adsorption–desorption isotherms and the corresponding pore size distributions of BaO pure and ZnO pure, ZnBaO and ZnBaCaO samples respectively photocatalysts. According to the Brunauer–Deming–Deming–Teller classification, the isotherms of all prepared samples are of type II and a small hysteresis behavior occurs. Such fact demonstrates that a large quantity of agglomerated particles reacts by a diffusion process, decreases the porosity and forms large particles [75].

The BJH distribution plot (inset of Figure 4.4.a) of BaO shows the presence of a unique pore size distribution peak centered at ~12.5 nm. This result indicates the mesoporous nature of the prepared BaO pure.

In the other hand, the pore size distributions (inset of Figure 4.4.b) are very broad (centered at forZnO: 40nm, ZnBaO: 60 nm and ZnBaCaO: 80nm), further confirming the presence of large mesopores and macropores. Considering the absence of a pore structure inside the individual nanoparticles on the basis of SEM results, these pores can be related to the pores between the aggregated prepared photocatalysts particles.

The ZnBaO sample shows a clear decreasing specific surface area, on the contrary of that of the ZnBaCa sample, which are listed in Table 4.1. This is because the BaO pure sample has the smallest particle size, whereas the ZnBaCaO sample has the largest particle size.
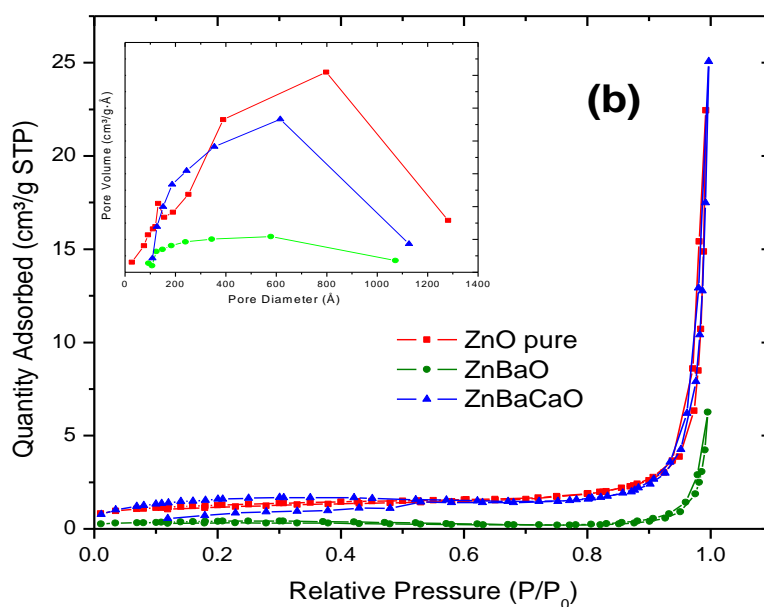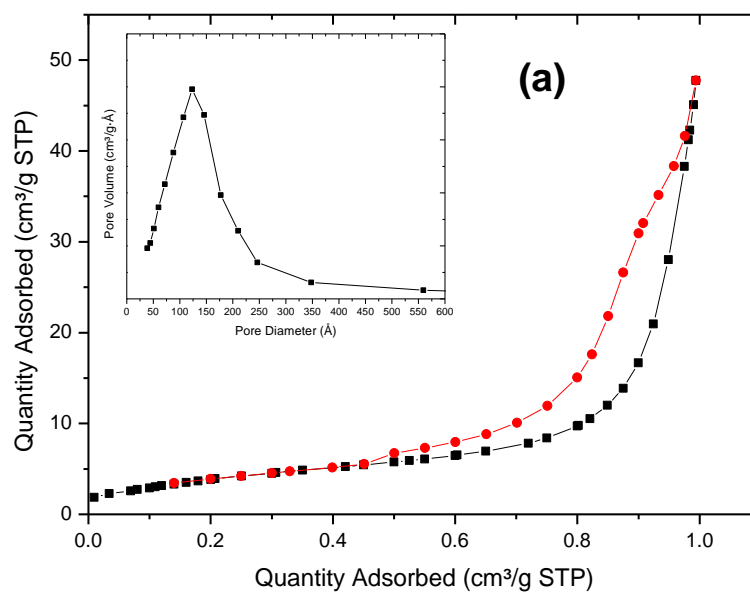
Figure 4.4: Nitrogen adsorption-desorption isotherms and corresponding pore size distribution curves (inset) of (a) BaO pure and (b) ZnO pure, ZnBaO and ZnBaCaO samples.

4.2. Malachite Green (MG) calibration

For the determination of the MG model dye concentration (used for the photocatalytic degradation tests) by UV-visible spectrometry a calibration was first done at maximum wave length of 618 nm. From this calibration presented in the figure.4-1, the extension coefficient

to be used in the beer- Lambert equation obtained from the slope was find to be equal to 0.1346 $L.mg^{-1}.cm^{-1}$.
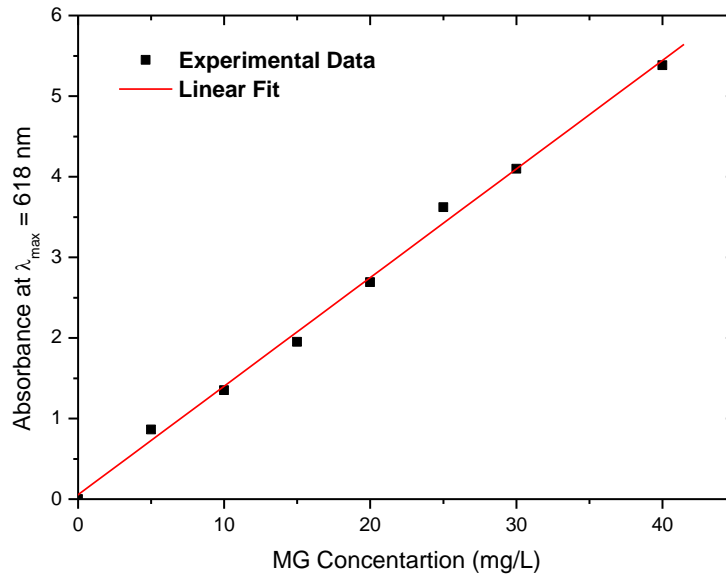
Figure.4.5: Malachite Green Calibration by UV- Visible spectrometry at 618 nm maximum wavelength

4.3. Malachite Green dark adsorption

Prior to the photocatalytic degradation, a very important step in the heterogeneous photocatalysis reaction has to be done. This step is the adsorption in the dark of the molecule to be degraded until saturation. The study of this step provides very important information on the ultimate adsorbed amount and the kinetic of the adsorption reaction.
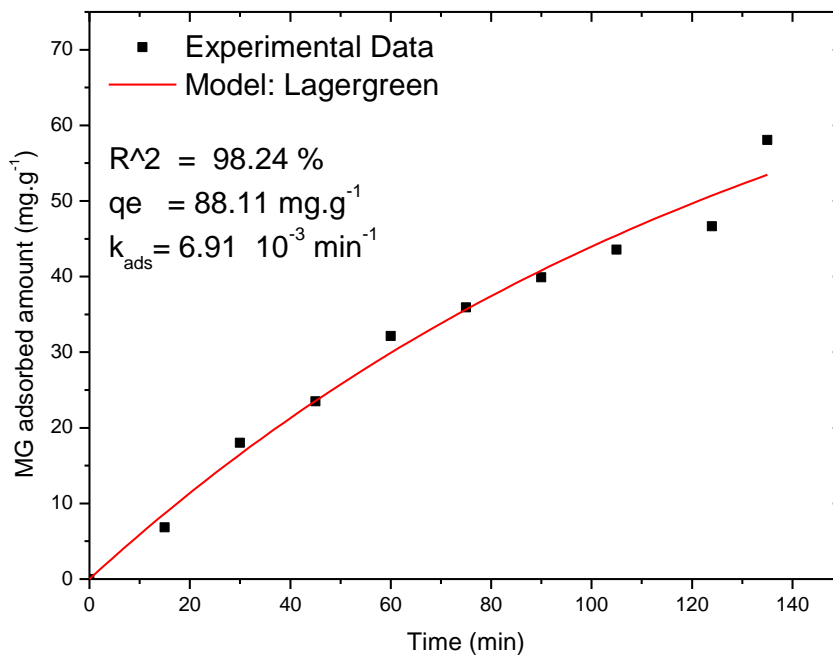
4.3.1 Adsorption Kinetics

Figure 4.6 shows the kinetic of MG adsorption on the ZnBaO photocatalyst in the dark. As can be clearly seen, the experimental data obeys to the Lagergren first order model given by the equation:

$$q = qe_x(1 - \exp(-k_{ads_x}t)) \tag{2}$$

Where q and qe (in mg/g) are respectively the adsorbed amount at time t and at equilibrium and k_{ads} is the kinetic constant of the adsorption reaction.

The values of the adsorption kinetic constant and the adsorbed amount at equilibrium determined by the Lagergren model are listed in the figure 4.6 and the table 4.2.

Figure 4.6: Kinetic of MG adsorption on the ZnBaO photocatalyst in the dark

### 4.3.2. Adsorption isotherms

The adsorption isotherms relate the specific relation between the adsorbate concentration and its degree of accumulation onto adsorbent surface at the constant temperature. Various isotherm models can be used to fit to the experimental data and evaluate the isotherm performance for MG adsorption. From these isotherm models we select the most used in liquid phase namely the Freundlich model [24] and the Langmuir model [25].

Freundlich Model: $qe = K_{Fx} Ce^{(1/n)}$ **(3)**

Langmuir Model: $qe = (q_{max\ x} K_{Lx}Ce)/(1 + K_{Lx}Ce)$ **(4)**

Where qe and q_{max} (in mg/g) are respectively the adsorbed amount at equilibrium and maximum, K_F (in $(L/mg)^{1/n}$) and K_L (in L/mg) are the Freundlich and Langmuir constant respectively and n is the Freundlich second parameter.

The adsorption plots and the fitting model parameters with R2 for the two used models are shown in Figure.4.7. In terms of R2 values, the applicability of the above two models for present experimental data approximately followed the order: Langmuir > Freundlich. It can be concluded that the Langmuir equation has the best fit to the experimental data. The maximum adsorption capacity calculated by this function is 221.10 mg/g and the Langmuir adsorption equilibrium constant is 10.06 10^{-3} L/mg.
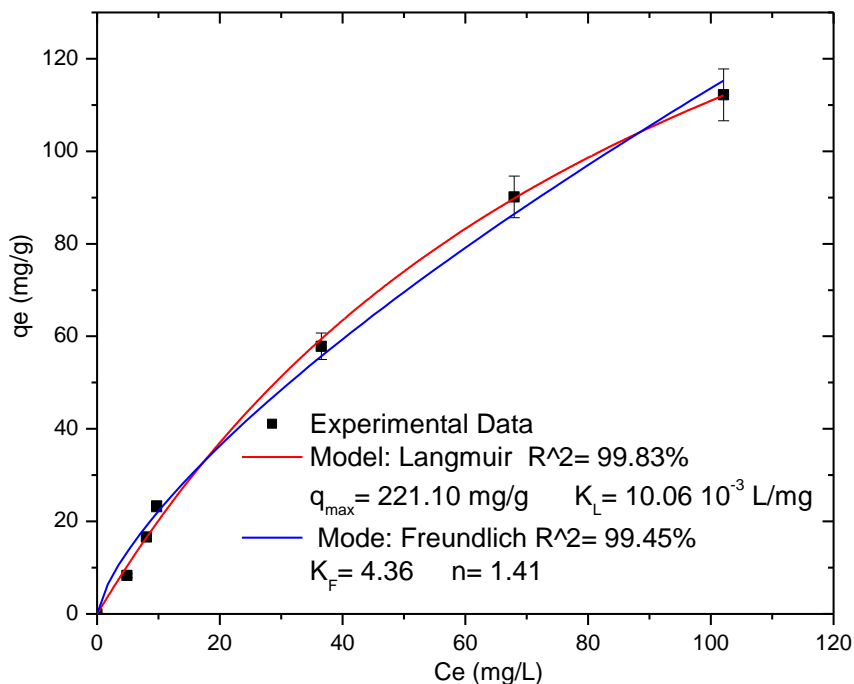
Figure 4.7: Adsorption plots and the fitting Langmuir and Freundlich models parameters with correlation coefficients R2

4.4. Kinetics study for photocatalytic degradation of Malachite Green

Photocatalysis degradation of MG is attributed to heterogeneous catalytic interaction between adsorbed MG and photocatalyst, and the oxidation reaction occurs due to the presence of OH radicals generated from the reaction between photocatalyst and H_2O under UV or visible irradiation. Usually the advanced oxidation process is greatly affected by many parameters such as: the nature of the substrate as well as the catalyst concentration, the pH of the suspension and the zero point charge of the catalyst, etc.

Studying all of these parameters takes a very long time that is why we limit our work to the degradation kinetics study of MG in simple conditions.

Figure.4.8. exhibits the degradation kinetics of MG in the presence of the different prepared photocatalysts. The excellent fits of experimental data obtained suggest that the MG degradation follows the pseudo first-order kinetics for all photocatalysts. The apparent rate constant k_{app} and the correlation coefficient R2 for the kinetics of MG are given in Table 4.2.

.
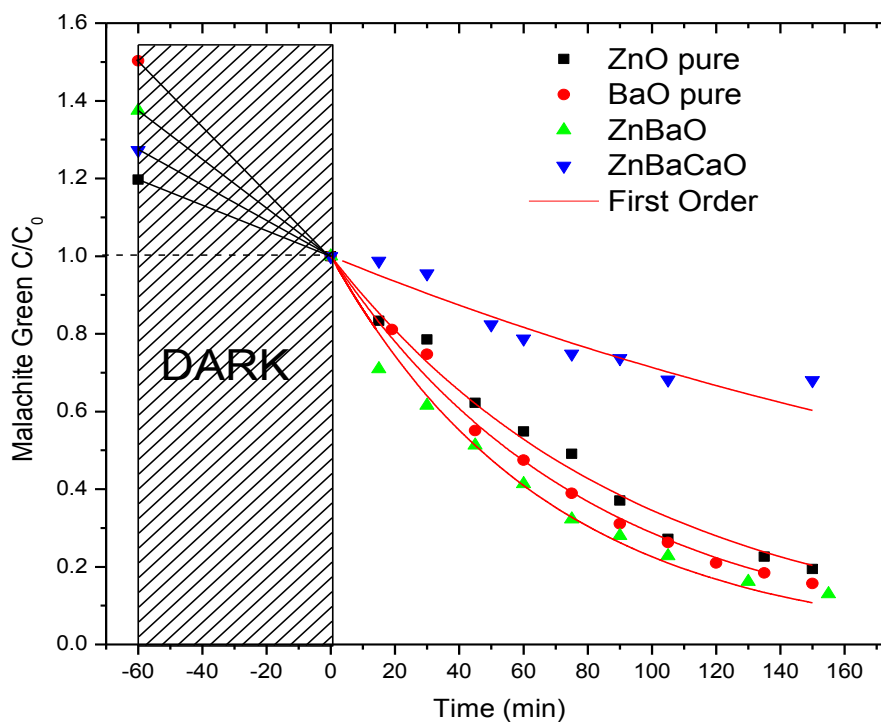
Figure.4.8: Photocatalytic degradation curves of MG with the prepared photocatalysts under visible irradiation

From the figure 4.9. (a) and (b) it is clear that the most active prepared photocatalyst for the Mg degradation under visible irradiation is the Ba doped ZnO (ZnBaO). In fact the apparent degradation kinetic constant decreases in the order: ZnBaO > BaO > ZnO pure > ZnBaCaO. However, taking in account the photocatalysts specific surface areas, the order is slightly changed but the intrinsic photoactivity ($min^{-1}.g/m^2$) of ZnBaO is at least 14 times higher proving that even if the surface is a very important parameter, the heterogeneous photocatalysis is a much more complex phenomenon.
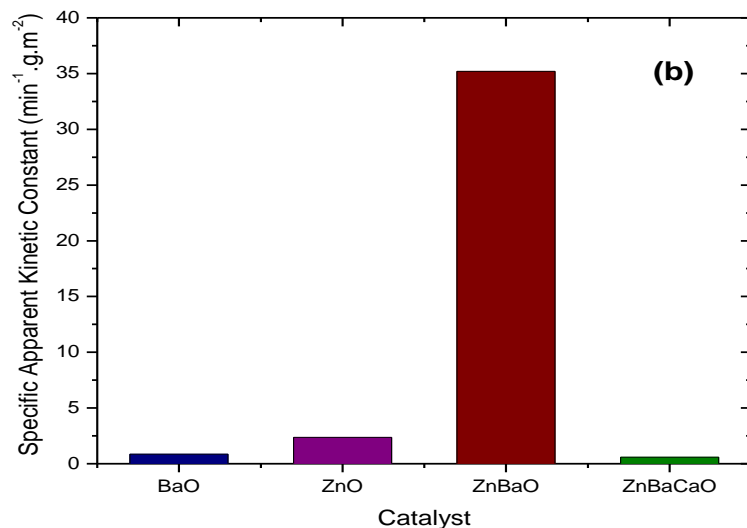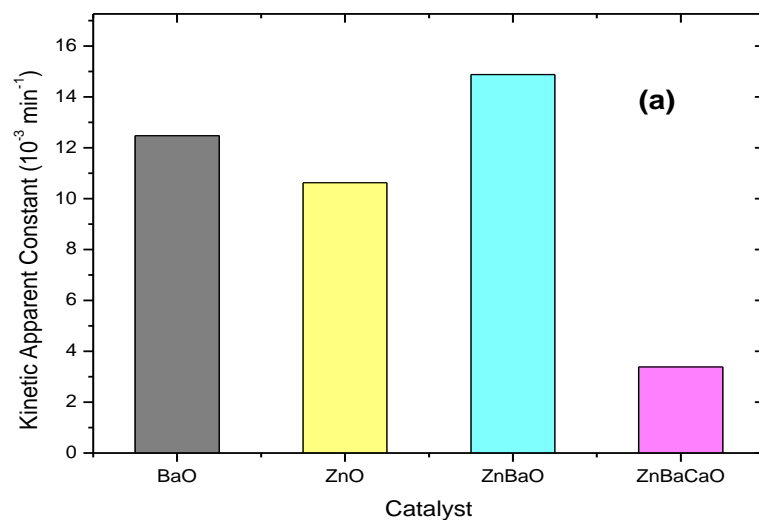
Figure.4.9: Photocatalytic degradation curves of MG with the prepared photocatalysts under visible irradiation

Table4.2. Structural parameters of prepared photocatalysts

Samples	MG Adsorption			MG Degradation		
	k_{ads} $(10^{-3}\ min^{-1})$	q_e (mg/g)	Adsorption amount %	k_{app} $(10^{-3}\ min^{-1})$	R2 %	S_{BET} $(m^2.g^{-1})$
BaO pure			50.00	12.48	99.30	14.51
ZnO pure			27.37	10.62	98.65	4.51
ZnBaO	6.91	88.11	34.47	14.88	98.43	1.45
ZnBaCaO			19.79	3.38	95.26	5.82

Chapter 5
CONCLUSION

Pure Zinc oxide, pure Barium oxide, Barium doped zinc oxide and barium- calcium co-doped zinc oxide nanoparticles have been synthesized using co-precipitation method.

The X-ray diffraction study confirmed that the prepared particles were of the cubic structure for BaO and of the hexagonal wurtzite structure for the other prepared nanoparticles, and the particles sizes were estimated. The isotherms of all prepared samples are of type II, indicating the presence of mesopores (30–100 nm) with small hysteresis behavior. Adsorption reaction of Malachite Green (MG) follows the Lagergren pseudo first order kinetic band obeys to Langmuir model. The photoactivity measurements were performed by monitoring the degradation of malachite green in solution under visible light using a batch setup. From the photoactivity, there was an increase in the malachite green degradation rate with the doping of zinc oxide with 1mol.% barium. This was unexpected based on the lowest specific area of this photocatalyst (ZnBaO) suggesting that heterogeneous photocatalysis is not only a matter of high surface area and adsorption.

REFERENCES

[1] Agriculture and water, Information Office of the Royal Embassy of Saudi Arabia in Washington, DC, 2013

[2] Al-Zahrani K. H.; Baig M. B., The Journal of Animal & Plant Sciences, (2011), 21(3): pp. 601-604,

[3] Ministry of Water and Electricity, "Supporting Documents for King Hassan II Great Water Prize", 2012

[4] M.Yahia et H.Batis ; Eur.J.Inorg.Chem. ; 2486-2494 ; 2003.

[5] J.Ye, Z.Zou et A.Matsushita ; I.J.Hydrogen Energy ; 28 ; 651-655 ; 2003.

[6] Y.Yokoi, I.Yasuda, H.Uchida, O.Okada, Y.Nakamura, H.Ishikawa et   H.Kimura ;
    ″Studies in Surface Science and Catalysis″ 130; 1319-1323 ;

[7] K.H.Felgner, T.Muller, H.T.Langhammer, H.P.Abicht ; Mater.Lett.; 58 ;
    1943-1947 ; 2004.

[8] A.F.Reid et M.J.Sienko ; Inorg.Chem. ; 6(3) ; 521-524 ; 1967.

[9] A.Varez, M.T.F.Diaz, J.Sanz ; J.Solid State Chem. ; 177 ; 4665-4671 ; 2004.

[10] S.Ben Aissa ; Diplome des études approfondies en chimie industrielle ; Institut
    national des sciences appliquées ; 8 ; 2004.

[11] Z.Ding, M.Zhang et J.Han ; Mater.Phys.Mech. ; 4 ; 107-110 ; 2001.

[12] J.L.Sotelo, G.Ovejero,F.Martinez, J.A.Melero et A.Milieni ; Appl.Catal.B ; 47(4) ;
    281-294 ; 2004.

[13] S.Irusta, M.P.Pina, M.Menendez et J.Santamaria ; J.Catal ; 179 ; 400-412 ; 1998.

[14] D.M.A.Melo, A.Cesar, A.E.Martinelli, Z.R.Silva, E.R.Leita, E.Longo et
    P.S.Pizanni ; J.Solid State Chem. ; 177 ; 670-674 ; 2004.

[15] J .P.Attfield ; I.J.Inorg.Mater. ; 3 ; 1147-1152 ; 2001.

[16] M.Alifanti, J.Kirchnerova, B.Delmon et D.Klavana ; Appl.Catal.A ; 262(2) ; 167-
    176 ; 2004.

[17] Z.Liu, B.Guo,L.Hong et H.Jiang ; J.Phys.Chem.Sol. ; 66 ; 161-167 ; 2005.

[18] H.Tanaka, N.Mizuno, M.Misono ; Appl.Catal.A ; 244 ; 371-382 ; 2003

[19] C. W. BUNN Proc. Phys. Soc. 47 (1935) 835.

[20] D.G. Thomas, J. Phys. Chem. Solids, 15 (1960) 86.

[21] I. Horner, J. Haufe, Chem. Ber., 101 (1968) 2921.

 [22] E. H. KISI, M. M. ELCOMBE, Acta. Cryst., 45 (1989)1867.

[23] A. Ashrafi, C. Jagadish, J. Appl. Phys., 071101 (2007) 102.

[24] A. Segura, J. A. Sans, F. J. Manjon, A. Munoz, M. J. Herrera-Cabrera, App. Phys. Lett., 83 (2003) 278.

[25] Muhammad Z. Ahmad, Jin Chang, Muhammad S. Ahmad, Eric R. Waclawik, Wojtek Wlodarski, Sens. Actuato. B 177 (2013) 286.

[26] S.J. Pearton, D.P. Norton , K. Ip, Y.W. Heo, T. Steiner, Progr. Mater. Sc. 50 (2005) 293.

[27] Handbook of Chemistry and Physics, 56th Edition, Ed. R.C. Weast, CRS Press (1975).

[28] W. Li, D. Mao, F. Zhang, X. Wang, X. Liu, S. Zou, Q. Li and J. Xu, Nucl. Instrum. Methods. Phys. Res. B, 169(2000) 59.

[29] Z.L. Wang J. Song, Scien., 312 (2006), 242.

[30] M. Miyauchi, A. Nakajima, T. Watanabe, K. Hashimoto, Chem. Mater. 14 (2002) 2812.

[31] A. Akyol, M. Bayramoglu, J. Hazard. Mater. B 124 (2005) 241.

[32] N. Daneshvar, D. Salari, A.R. Khataee, J. Photochem. Photobiol. A: Chem. 162 (2004) 317.

[33] R. Comparelli, E. Fanizza, M.L. Curri, P.D. Cozzi, G. Mascolo, G. Agostiano, Appl. Catal. B: Environ. 60 (2005) 1.

[34] H.C. Yatmaz, A. Akyol, M. Bayramoglu, Ind. Eng. Chem. Res. 43 (2004) 6035.

[35] S. Su, S.X. Lu, W.G. Xu, Mater. Res. Bull. 43 (2008) 2172.

[36] A. Sharma, P. Rao, R.P. Mathur, S.C. Ameta, J. Photochem. Photobiol. A 86 (1995) 197.

[37] V. Kandavelu, H. Kastien, K.R. Thampi, Appl. Catal. B: Environ. 48 (2004) 101.

[38] P. Percherancier, R. Chapelon, B. Pouyet, J. Photochem. Photobiol. A: Chem. 87 (1995) 261.

[39] A.A. Khodja, T. Sehili, J.F. Pihichowski, P. Boule, J. Photochem. Photobiol. A: Chem. 141 (2001) 231.

[40] I. Poulios, M. Kositzi, A. Kouras, J. Photochem. Photobiol. A: Chem. 115 (1998) 175.

[41] J. Domenech, A. Prieto, J. Phys. Chem. 90 (1986) 1123.

[42] N. Kislov, J. Lahiri, H. Verma, D.Y. Goswami, E. Stefanakos, M. Batzill, Langmuir 25 (2009) 3310.

[43] L.B. Khalil, W.E. Mourad, M.W. Rophael, Appl. Catal. B 17 (1998) 267.

[44] F.D. Mai, C.C. Chen, J.L. Chen, S.C. Liu, J. Chromatogr. A 1189 (2008) 355.

[45] S. Navarro, J. Fenoll, N. Vela, E. Ruiz, G. Navarro, J. Hazard. Mater. 172 (2009) 1303.

[46] B. Pare, S.B. Jonnalagadda, H. Tomar, P. Singh, V.W. Bhagwat, Desalination 232 (2008) 80.

[47] S. Sakthivel, B. Neppolian, M.V. Shankar, B. Arabindoo, M. Palanichamy, V. Murugesan, Sol. Energy Mater. Sol. Cells 77 (2003) 65.

[48] S.K. Pardeshi, A.B. Patil, Sol. Energy 82 (2008) 700.

[49] S. Daniele, M.N. Ghazzal, L.G. Hubert-Pfalzgraf, C. Duchamp, C. Guillard, G. Ledoux, Mater. Res. Bull. 41 (2006) 2210.

[50] M. El-Kemary, H. El-Shamy, I. El-Mehasseb, J. Lumin. 130 (2010) 2327.

[51] G. Colón, M.C. Hidalgo, J.A. Navío, E. Pulido Melián, O. González Díaz, J.M. Dona Rodríguez, Appl. Catal. B 83 (2008) 30.

[52] R. Velmurugan, M. Swaminathan, Sol. Energy Mater. Sol. Cells 95 (2011) 942.

[53] V. Shinde, T.P. Gujar, T. Noda, D. Fujita, A. Vinu, M. Grandcolas, J. Ye, Chem. Eur. J. 16 (2010) 10569.

[54] F. Xu, P. Zhang, A. Navrotsky, Z.-Y. Yuan, T.-Z. Ren, M. Halasa, B.-L. Su, Chem. Mater. 19 (2007) 5680.

[55] Y. Wang, X. Li, N. Wang, X. Quan, Y. Chen, Sep. Purif. Technol. 62 (2008) 727.

[56] O.Y. Khyzhun, V.L. Bekenev, V.V. Atuchin, E.N. Galashov, V.N. Shlegel, Mater. Chem. Phys. 140 (2013) 588.

[57] Abdessalem Hamrouni, Hinda Lachheb, Ammar Houas., Journal : Materials Science and Engineering B 178 (2013) 1371– 1379

[58] Abdessalem Hamrouni, Noomen Moussa, Francesco Parrino, Agatino Di Paolab, Ammar Houas, Leonardo Palmisano., Journal of Molecular Catalysis A: Chemical 390 (2014) 133–141

[59]. Abdessalem Hamrouni, Noomen Moussa, Agatino Di Paolab, Francesco Parrino, Ammar Houas, Leonardo Palmisano., Applied Catalysis B: Environmental 154–155 (2014) 379–385

[60] Abdessalem Hamrouni, Noomen Moussa, Agatino Di Paola, Leonardo Palmisano, Ammar Houas, Francesco Parrino, Journal of Photochemistry and Photobiology A: Chemistry, 309 (2015) 47-54

[61] Abdessalem Hamrouni, Noomen Moussa, Agatino Di Paola, Francesco Parrino, Ammar Houas, Leonardo Palmisano, Applied Catalysis B: Environmental, Volumes 154–155 (2014), 379-385

[62] D. G. Thomas, J. Phys. Chem. Solid., 3 (1957) 229.

[63] A. Hausmann, B. Utsch Z. Phys. B 21(1975) 217.

[64] G. Neumann, Curr. Topic. Mater. Sc., 7 (1981)152.

[65] A. Janotti, C. G. V. Walle, Appl. Phys. Lett., 87 (2005)102.

[66] A. Janotti, C. G. V. Walle, J. Cryst. Grow., 58 (2006) 287.

[67] A. Janotti, C. G. V. Walle, Phys. Rev. B, 75 (2007)165.

[68] A. Janotti, C. G. V. Walle, Rep. Prog. Phys. 72 (2009) 12650.

[69] D. P. Norton, Y. W. Heo, M. P. Ivill, K. Ip, S. J. Pearton, M. F. Chisholm, T. Steiner, mat. tod., 7 (2004) 34.

[70] J. M. Herrman, Appl. Catal. B: Envir., 99 (2010) 461.

[71] J. M. Herrman, Catal. Today, 53 (1999) 115.

[62] G. Palmisano, V. Augugliaro,M. Pagliaro, L. Palmisano, Chem. Commun., 0 (2007) 3425.

[73] S. Goldstein, G. Czapski, J. Rabani, J. Phys. Chem., 98 (1994) 6586.

[74] G.U. Buxton, C.L Greenstock, W.P. Helman, A.B. Ross, J. phys. Chem. Ref. Data, 17 (1988) 513.

[75] Nasar, R. S.; Cerqueira, M.; Longo, E.; Varela, J. A. Cerâmica. 2008, 54, 38.

CURRUCLUM VITAE